THE JOURNAL OF PHYSICAL CHEMISTRY C

Article

Cite This: J. Phys. Chem. C 2019, 123, 10237−10245

pubs.acs.org/JPCC

Lithium Diffusion Mechanism through Solid−Electrolyte Interphase in Rechargeable Lithium Batteries

Ajaykrishna Ramasubramanian, Vitaliy Yurkiv, Tara Foroozan, Marco Ragone, Reza Shahbazian-Yassar, and Farzad Mashayek*

Department of Mechanical and Industrial Engineering, University of Illinois at Chicago, Chicago, Illinois 60607, United States

Supporting Information

ABSTRACT: The composition, structure, and the formation mechanism of the solid−electrolyte interphase (SEI) in lithium-based (e.g., Li-ion and Li metal) batteries have been widely explored in the literature. However, very little is known about the ion transport through the SEI. Understanding the underlying ion diffusion processes across the SEI could lead to a significant progress, enabling the performance increase and improving safety aspects of batteries. Herein, we report the results of first-principles density functional theory calculations on the dominant diffusion pathways, energetics, and the corresponding diffusion coefficients associated with Li diffusion through the polycrystalline SEI. This paper is particularly concerned with the Li diffusion through the grain boundary (GB) formed between the three major inorganic components of the SEI, such as Li_2O, LiF, and Li_2CO_3. It is found that Li diffusion occurs through the numerous open channels formed by the GB. The energetics and potential barriers vary significantly depending upon the structure of these channels, with the general trend being that Li diffusion in the GB is generally faster than in the neighboring crystalline regions within the grain interiors. In addition, the elastic properties of the GB are calculated allowing for more profound understanding of the SEI stability and formation.

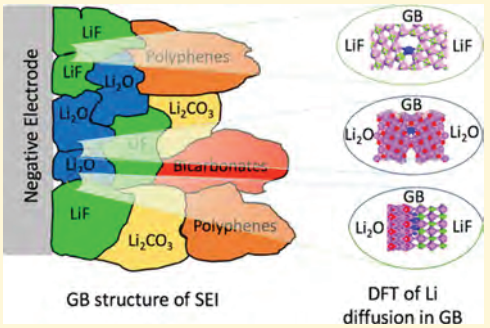

1. INTRODUCTION

Lithium-based batteries, such as Li-ion batteries (LIBs) and Li metal batteries (LMBs), are widely used as power sources for a variety of applications starting from small portable (e.g., phones, laptops, etc.) up to automotive, unmanned aerial vehicles and grids. However, still further improvements are expected for their widespread usage in high-power devices.[1−3] During battery operation, a thin (nanoscale) solid−electrolyte interphase (SEI) film grows on the surface of an electrode as a result of the decomposition of an electrolyte. It is generally believed[4−6] that the SEI provides many beneficial functions to the battery operation, one of which is by controlling Li uniform delivery to the electrode surface, where the charge-transfer reaction occurs. However, as the SEI further grows and expands, numerous defects and grain boundaries (GBs) are formed, leading to a significant anisotropic diffusivity of Li toward the electrode surface. This results in an uneven Li delivery to the electrode/SEI interface, leading to undesired phenomena, which cause performance decrease and possibly failure of a battery. These phenomena include random Li electrodeposition and dendrite formation in LMBs and anisotropic diffusion/reaction and exfoliation in the case of LIBs.

The concept of the SEI was first introduced by Peled[7] in 1979 and further improved in their later works.[8−10] With further contributions to the field of the SEI understanding,[11−17] two major models have emerged explaining the SEI structure and composition. The first model is called "multi-component, multilayer structure"[18] and the second model, developed by Shi et al.,[19] is called "two-layer-two-mechanism diffusion". Both models describe the SEI as a two-layer film consisting of organic (outer layer—close to the electrolyte) and inorganic (inner layer—close to the electrode). The main difference between these two models lies in the structure of the inner layer. In particular, the first model describes it as a grain-structured layer, where ions can diffuse through the grains (i.e., the individual components of the SEI) and the GB formed between these individual components. The second model considers the inner layer as one structured sublayer, where ions diffuse through it via the knock-off mechanism.[19] Because the inner (inorganic) layer is located directly at the surface of the negative electrode, the ion diffusion through this last layer directly affects the morphology of Li electrodeposition and governs the cycling performance of the battery.

Although many studies[14,20,21] have been performed to understand parameters such as composition, morphology, and thickness of the SEI and their growth mechanisms, very little effort was made to understand the SEI as an ion transport medium and the role of GB diffusion. This is due, in part, to the fact that the experimental verification of such theories is very challenging. Moreover, most of the SEI components are highly reactive when exposed to contaminants, air, or

Received: January 15, 2019
Revised: March 27, 2019
Published: March 29, 2019

DOI: 10.1021/acs.jpcc.9b00436
J. Phys. Chem. C 2019, 123, 10237−10245

humidity.[14] For these reasons, the ex situ characterization of the SEI becomes very difficult, whereas in situ experiments require specially designed tools and precise characterization tools.[22] Given the difficulties of experimental techniques, computational simulations,[23] especially using ab initio density functional theory (DFT),[24−27] have become a valuable tool to study the properties and diffusion characteristics of the SEI. Thus, in this study, we focus on the GB of the SEI employing DFT in an effort to understand and evaluate the diffusion pathways and energetics of Li transport. Figure 1 illustrates the

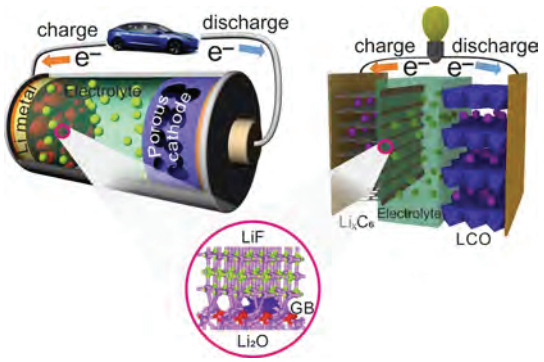

Figure 1. Schematic illustration of the SEI envisioned in the present work. Upper left picture depicts a LIM showing the SEI on the Li−metal surface; upper right picture depicts a graphite-based LIB with the SEI; lower picture shows the atomic structure of a representative GB, which is a focus of this paper. Note: all drawings shown in this picture are not to scale merely for illustrative purpose.

emphasis of this work showing a Li−metal cell highlighting the exaggerated SEI structure (red bubble-like structures in the upper left picture), a graphite-based anode Li-ion cell highlighting the exaggerated SEI structure (upper right picture), and the atomic structure of the GB formed between two representative components of the inner layer of the SEI (lower picture). Using the DFT method, this paper concentrates specifically on the Li diffusion through the GB of the inner layer and the stability of different GBs.

Before developing the detailed concept of the Li diffusion model through the SEI, it is helpful to review the aspects of the Li diffusion through the SEI individual components. The major components of the inner inorganic layer of the SEI in both the Li metal and graphite negative electrodes are lithium fluoride (LiF), lithium oxide (Li_2O), and lithium carbonate (Li_2CO_3) at temperatures in the range of 250−400 K. Benitez et al.[28] have used the classical molecular dynamics (MD) simulations to study the Li-ion diffusivity in three main inorganic components of the SEI. They found that vacancy-assisted and knock-off diffusion in LiF, direct ion-exchange mechanism in Li_2O, and vacancy and knock-off mechanism in Li_2CO_3 are the dominant mechanisms. Shi et al.[29] calculated the Li-ion diffusion in Li_2CO_3 via a "knock-off" mechanism, assuming that the inorganic layer of SEI is Li_2CO_3. In addition, they identified the dominant diffusion carrier in Li_2CO_3 at different voltage ranges. Soto et al.[30] employed ab initio MD to better understand the diffusion of both Li and Na ions in the SEI components such as LiF, Li_2CO_3, NaF, and Na_2CO_3. They showed that the Li ions in Na-based SEI components prefer an interstitial ion diffusion through the knock-off or direct hopping mechanism, whereas the Na ions in Li-based SEI components show a preference for the vacancy diffusion and knock-off mechanisms.

Liu et al.[25] have performed DFT calculations to evaluate the influence of two major SEI components (LiF and Li_2CO_3) on the Li surface energy. Their study shows that the LiF/Li interface has higher electron tunneling energy barrier from the Li metal to SEI than the Li_2CO_3/Li interface. In the other study, Chen et al.[31] calculated the Li migration energy barriers along major diffusion pathways and energy barriers of the three main components (Li_2CO_3, Li_2O, and LiF) of the inner SEI layer using DFT. Yildrim et al.[24] have applied first-principles calculation to study defect thermodynamics, the dominant diffusion carriers, and the diffusion pathways in crystalline LiF and NaF components of the SEI. They reveal that for both compounds, vacancy defects are energetically more favorable; therefore, they form more readily than interstitials because of the close-packed nature of the crystal structures. However, the vacancy concentrations are very small for the diffusion processes facilitated by defects.

The works of Peled et al.,[10] Christensen and Newman,.[32] and recently Leung and Jungjohann.[33] are the only studies providing information on details of diffusion through GB in the SEI. Peled et al.[10] provided evidence for Li transport via the SEI GBs through impedance analysis and calculation of the apparent SEI ionic resistance. Christensen and Newman,[32] on the other hand, developed a mathematical model to simulate the growth of the SEI and transport of lithium and electrons through the film via vacancies and interstitials and also concluded that GBs and diffusion through them might be an important factor. Leung and Jungjohann.[33] have used the DFT calculation to reveal that Li_2O GBs of the SEI with sufficiently large pores can accommodate Li^0 atoms. Also, they showed that Li−metal nanostructures as thin as 12 Å are thermodynamically stable inside Li_2O cracks. Subsequently, these Li nanostructures become Li filaments.

To date, there is no work dedicated to the detailed investigation of GB properties in the SEI and the Li diffusion through it. Thus, the present paper aims to fulfill this gap by providing a computational framework and the data necessary to understand Li diffusion in the GBs of the SEI.

The Methodology section provides the details of the computational methods that are utilized to capture the Li transport through the SEI. In Results and Discussion section, the results from our DFT calculations for different GBs are presented and are compared against the theoretical and experimental values that are calculated for the diffusion through the bulk crystal structures. In the Results section, our findings on stiffness properties and stabilities of these structures are first examined; the results from different GB combinations in the structures of SEI are then discussed; and finally, the details of the diffusion coefficients obtained through our DFT calculations are reported. In Summary and Conclusions section, the findings and conclusions are briefly summarized.

2. METHODOLOGY

The present DFT calculations are performed using the Vienna ab initio simulation package (VASP) code,[34] with the plane-wave basis sets and the projector augmented wave[35] pseudopotentials in the framework of Perdew−Burke−Ernzerhof sol[36] generalized gradient approximation.[37] The migration barriers are calculated using the nudged elastic band (NEB)[38] method as implemented in VASP. The NEB method

DOI: 10.1021/acs.jpcc.9b00436
J. Phys. Chem. C 2019, 123, 10237−10245

is an established technique for finding the minimum energy path (MEP) between the given initial and final states of a transition. Depending upon the configuration, there are five to nine images (structures) describing ion migration coordinates in the NEB calculations. For each diffusion coordinate, the maximum energy difference among all images is considered as the migration barrier for ionic diffusion. All images are simultaneously optimized along the diffusion path until the forces acting on the atoms in each image converged to 0.1 eV/Å.

To perform the NEB calculations, the ground-state lattice constants of the bulk structures are first calculated. Then using a slab method, where the *k*-point samplings are set based on the geometry of each structure for surface structure optimization, with one *k*-point in the surface normal direction defined with at least 15 Å vacuum region and the same number of *k*-points on the other two directions as in the bulk calculations, the surface energies of different possible surfaces are calculated. Additionally, in order to ensure that the slab thickness is chosen properly and represents the properties of the macroscopic crystal structure, the GB energy was calculated for two different slab thicknesses. In general, depending upon the system, the GB energy changed by ca. 2% compared with the increase of the slab thickness by ca. 10%. Thus, the minimum reasonable slab thickness is used.

The surface energy per unit area of a slab is the difference between the total energy of the relaxed slab structure and the bulk energy with the same number of atoms. The surface energy is given by

$$\gamma_{\text{surf}}^{\text{A}} = \frac{E_{\text{slab}}^{\text{A}} - N_{\text{A}}E_{\text{bulk}}}{S} \tag{1}$$

where $\gamma_{\text{surf}}^{\text{A}}$ is the surface energy of slab A, $E_{\text{slab}}^{\text{A}}$ is the total energy of the relaxed slab, E_{bulk} is the energy of the bulk per unit structure of A, N_{A} is the number of units of A, and S is the surface area.

Because the minimum energy surfaces are generally the most stable and naturally formed surfaces in the grain structure, these surfaces are then cleaved to form the GBs and are optimized. Using the optimized ground-state GB structure, the GB energy is evaluated. The GB energy is calculated as follows

$$\gamma_{\text{GB}} = \frac{E_{\text{GB}}^{\text{AB}} - N_{\text{A}}E_{\text{A}} - N_{\text{B}}E_{\text{B}}}{2S} \tag{2}$$

where γ_{GB} is the GB energy; $E_{\text{GB}}^{\text{AB}}$ is the total energy of the relaxed GB structure; E_{A} and E_{B} are the bulk energies of structures A and B; N_{A} and N_{B} are the number of unit cells of A and B, respectively; and S is the surface area of the interface.

Because the knowledge of elastic properties allows to assess the mechanical stability of the studied systems,[39,40] it is imperative to evaluate the elastic properties of the GB systems. The elastic constants are computed by the stress−strain method outlined in Yu et al.,[41] and all atomic positions are fully relaxed when simulating the application of external strains. This method follows a well-established procedure of evaluating the components of the elastic tensor by computing the first derivative of the stresses calculated in VASP, rather than evaluating the second derivatives of the total energy with respect to strain.

After identifying both the thermodynamically and mechanically stable GBs, the lithium diffusion channels through them are identified, and the NEB calculations are performed to obtain the migration barrier for Li to diffuse in that channel. The calculated values of the migration barriers are then used as the activation energies to calculate the diffusion coefficients. The diffusion coefficient is calculated by the Arrhenius equation

$$D = D_0 \exp\left(-\frac{E^{\text{act}}}{k_{\text{B}}T}\right) \tag{3}$$

where the pre-exponential factor $D_0 = ga^2\nu$; g is the dimensionality (1−3); a is the migration distance taken from the NEB path; and ν is the attempt frequency (10^{13} s^{-1}). The value of attempt frequency is used as a standard value for the first-order reaction, in which the entropy of the transition state does not notably differ from that of the initial diffusion position in the ground state. E^{act} is the activation energy, k_{B} is the Boltzmann constant, and T is the temperature.

All the simulation cells considered are overall charge neutral. A 400 eV plane-wave energy cutoff is imposed. In general, depending upon the GB structure, the further increase of cutoff to 450 eV led to the change of the total energy of less than 0.1 meV. The forces on atoms were reduced to under 1 meV/Å. The criterion for energy change is set to 0.1 meV. In calculations of odd number of Li atoms in the simulation cell, spin-polarized DFT is applied. Depending on the investigated system, the appropriate smearing method is used.

3. RESULTS AND DISCUSSION

3.1. GB Creation. As explained in the Methodology section, first the bulk structures, as shown in Figure S1 (Supporting Information A), of LiF (8 atoms), Li_2O (12 atoms), and Li_2CO_3 (24 atoms) are created and their bulk energies are calculated. Then the vacuum slabs with different surface orientations are formed, as shown in Figure S2 (Supporting Information A), to calculate the surface energies and thereby identify the most stable surface for the GB interface. In Table 1, the calculated surface energies of different surface orientations of the SEI components are listed and also compared against the existing literature. From the surface energy values, we can infer that the most stable and energetically favorable surfaces for Li_2O, LiF, and Li_2CO_3 have the (111), (001), and the (001) orientations, respectively. Although the (001) surface of Li_2CO_3 has a very low energy (11.85 meV/Å^2), it does not form the stable GBs because they readily reduce electrochemically in the presence of Li.[33] In addition, the aging of electrodes,[45,46] electrolyte-type,[47] and quality and the presence of hermetic seals[16] on the lithium-ion

Table 1. Surface Energies of Different Orientations of Major Inorganic SEI Components

		surface energies (meV/Å^2)	
SEI component	surface orientation	this work	from literature
LiF	(001)	21.84	20[42]
	(110)	51.18	49[42]
	(111)	54.17	55[42]
Li_2O	(100)	75.62	75[43]
	(110)	56.17	56[43]
	(111)	31.87	30[43]
Li_2CO_3	(001)	11.85	11.23[44]
	(110)	18.72	13.47[44]
	(110)	36.82	35.57[44]

DOI: 10.1021/acs.jpcc.9b00436
J. Phys. Chem. C 2019, 123, 10237−10245

cells may severely influence the presence and quantity of Li_2CO_3, therefore reducing the chances of forming a stable GB. Thus, the major GBs of interest are the GBs between LiF/LiF slabs, the GBs in Li_2O/Li_2O slabs, and the mixed GBs between LiF/Li_2O slabs. The GBs which contain single-crystal structures on either side are created using the coincident site lattice (CSL) theory.[48] The GBs are named using the symbol Σ based on the CSL theory as

$$\Sigma = \frac{\text{volume of CSL lattice}}{\text{volume of unit lattice}} \quad (4)$$

The atomistic tool kit[49−52] is used to build the GB, where the "Interface Builder" tool allows analyzing all possible GBs between two particular grains. The algorithm searches all possible repetitions and rotations of the two surfaces in order to find a common supercell with minimal strain. Because there are tens of possibilities between two different grains, we apply specific cutoff conditions, such as the GB width should be 2 Å and the strain of each surface should not be more than 5%. In addition, the natural limitation of the DFT method eliminates configurations with more than 300 atoms per GB. In this way, the most stable configurations for all GB will be identified and used in the followed-up tasks for Li diffusion study and mechanical property calculations.

3.1.1. LiF/LiF GB Creation. On the basis of the surface energy calculations, two kinds of the GB between LiF grains are constructed, that is, LiF (001) Σ3 (CSL volume: 195 $Å^3$) and Σ5 (CSL volume: 325 $Å^3$) GBs as illustrated in Figure 2a,b. The procedure for the GB creation is as follows. First, a LiF crystal at optimal lattice constants is rotated 18° and cleaved using the (001) surface to expose the (310) surface in the *x*-direction. A second, mirror-image slab is created by reflecting the first about the *x*−*y* plane. As shown in Figure 2a,b, there could be two possible structures based on the location of the mirror plane. The first structure is matched at the lattice point forming a closed GB structure and the second structure is achieved by the mirroring of the slabs slightly (about 1 Å) away from the coincident lattice points, which forms a slightly open GB structure. It should also be noted that the mirror or junction plane is a (310) plane of atoms common to both slabs, which is found to be energetically less favorable. Thus, the mirrored slab is shifted by half a lattice constant on the *z*-direction in order to achieve better stability and more coordination between Li and F atoms on either slab. The *z*-dimension of the cell is varied to introduce the vacuum of 18 Å to preclude interaction between slabs.

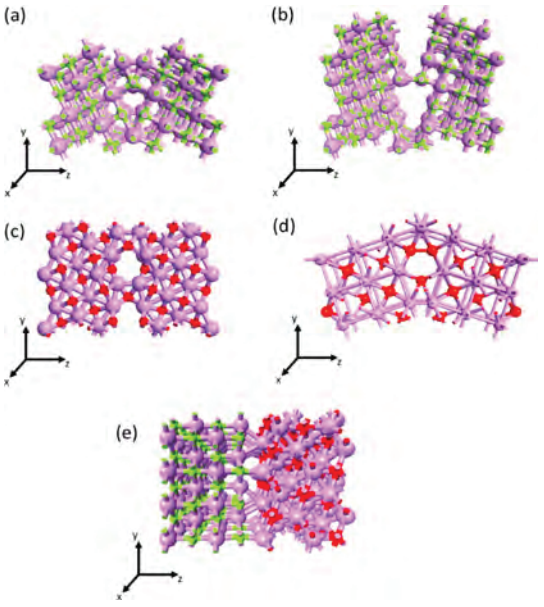

Figure 2. GB structures formed by LiF and Li_2O grains. (a) Compact LiF/LiF (310) GB (Σ3), (b) open LiF/LiF (310) GB (Σ5), (c) Li_2O/Li_2O Σ3 GB with the (111) oriented surface toward the interface, (d) Li_2O/Li_2O Σ15 GB with the (210) surface, and (e) $LiF(001)/Li_2O(111)$ GB structure. Pink colored spheres depict Li atoms, red colored spheres show F atoms, and red colored spheres illustrate O atoms.

3.1.2. Li_2O/Li_2O GB Creation. There are limited electronic structure studies of GBs in antifluorite lattice structures of AB_2 stoichiometry relevant to Li_2O. Similar to LiF/LiF GB, a simple Σ5 GB is created for Li_2O by joining (310) facets. However, in Σ5 configuration, one of its orthogonal surfaces is (001). This is the most stable surface for LiF but is a high energy surface for Li_2O. The lowest energy facet of Li_2O is (111). Because the Li_2O lattice structure is different from that of LiF, the model used in LiF is inapplicable, and the CSL approach has to be reapplied instead. On the basis of the CSL theory, taking the (111) direction as the *z*-axis, the Li_2O slab was mirrored by a plane that is 60° to the *x*−*y* plane and joined to form a Σ3 Li_2O (CSL volume: 303 $Å^3$) that has maximum Li−O contacts. This angle is chosen to give a modest system size with best lattice matching with the metal surface supercell. Similar to the Σ3 LiF GB, another structure could be achieved for the Li_2O GB using the (210) surface, mirrored with the *x*−*y* plane, forming a Σ15 GB (CSL volume: 1517 $Å^3$). Figure 2c,d shows both the achieved GB structures. Both GB structures are then optimized to their respective ground-state energies to evaluate the respective GB energies.

3.1.3. LiF/Li_2O GB Creation. Mixed LiF/Li_2O boundaries are created by joining the minimum energy surfaces of LiF and Li_2O, respectively, with minimum possible strain on either slab at the interface. In all cases, the *z*-direction is perpendicular to the GBs. From the surface studies, we calculated the most stable surfaces of LiF and Li_2O to be (001) and (111), respectively. The mixed LiF/Li_2O boundaries are created by joining the two surfaces of a LiF (001) slab onto Li_2O (111) slabs, as shown in Figure 2e. The good lattice matching of these two surfaces allows cations (Li^+) on one material surface to be coordinated to anions (F^- or O^{2-}) on the other and form a GB with a low strain value of 2.1% on either slab. The GB is oriented perpendicular to the *z* direction and the ion positions are optimized as in the previous cases.

From Table 2, we can infer that the elastic properties of the GBs have a direct correlation to the GB density. The GB density is evaluated as

$$\rho = \frac{2S}{abc} \quad (5)$$

where *S* is the surface area of the interface and *a*, *b*, and *c* are the lattice lengths of the supercell structure. Because the GB is oriented toward the *x*-direction, the value of *S* becomes $S = ab$, and the value of ρ becomes $\rho = 2/c$. It can be observed that as the GB density increases, the thickness of the grain when compared to the GB is increased and the stiffness of the material increases, but this value becomes significant only at very low GB densities (as low as 0.06[53]). Also, when compared to the microscale values of the bulk elastic modulus, a clear

DOI: 10.1021/acs.jpcc.9b00436
J. Phys. Chem. C 2019, 123, 10237−10245

Table 2. Summary of All the GB Structure Properties[a]

chemical system	supercell stoichiometry	*k*-points	γ_{GB} (mJ/m^2)	GB density (1/Å)	bulk modulus (GPa)
LiF/LiF (Σ5 GB)	$Li_{112}F_{112}$	5 × 3 × 1	380.79	0.130	76.88
LiF/LiF (Σ3 GB)	$Li_{68}F_{68}$	5 × 4 × 1	423.55	0.136	77.25
Li_2O/Li_2O (Σ3 GB)	$Li_{126}O_{63}$	5 × 5 × 1	688.72	0.166	65.79
Li_2O/Li_2O (Σ5 GB)	$Li_{102}O_{51}$	3 × 4 × 1	557.47	0.118	64.73
LiF/Li_2O	$Li_{120}F_{48}O_{36}$	3 × 3 × 1	288.62	0.124	64.22

[a]The first column shows the GB composition and notation, the second column shows the stoichiometry, the third column lists *006B*-point used in the present DFT calculations, the fourth column shows the calculated GB energies, the fifth column reports the GB density, and the last sixth column reports the calculated bulk modulus.

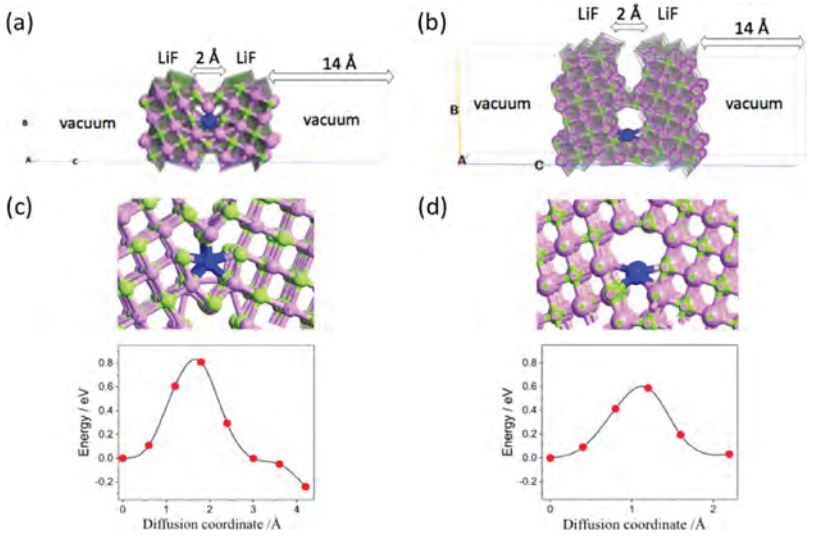

Figure 3. (a) Compact LiF/LiF (310) GB (Σ3) with Li adatom (marked in blue). (b) Open LiF/LiF (310) GB (Σ5) with Li adatom (marked in blue). (c) Migration barrier for compact LiF/LiF (310) GB (Σ3). (d) Migration barrier for compact LiF/LiF (310) GB (Σ3).

difference is observed owing to the small sizes of the SEI grain structures. For example, the reported bulk elastic modulus for Li_2O for microscale structures is 56 GPa, whereas the computed value for single-crystal Li_2O (4 nm) is 68 GPa.

Lower values of GB energy, γ_{GB}, indicate a stronger cohesive bonding between the two grains in contact. From the GB energy, γ_{GB}, it can be clearly identified that the Li_2O/Li_2O (Σ3 GB) structure is energetically much less favorable than the Li_2O/Li_2O (Σ15 GB). Furthermore, we also observed that the GB structure breaks apart when we add a Li adatom into the GB.

3.2. Li Diffusion through the GB. In this section, the results of the DFT calculations of Li diffusion through the above identified stable GB are presented. The activation energies (E^{act}) and pre-exponential factors are obtained, and respective diffusion coefficients are calculated. These results are then compared against the available experimental data and other computational results. This provides a better understanding on the interplay between the GBs in the SEI compounds and their effect on direction-dependent ion migration through the GB interface. There are three most common types of Li diffusion mechanisms, that is, hopping, knock-off, and vacancy-assisted diffusion, as identified in the prior literature[24,28,30] and reviewed in the Introduction section. In this work, we mainly observe multiatom hopping mechanism as shown in Figure S3. Because the GB between two adjacent grains creates an opening big enough for Li diffusion, the alternative knock-off and vacancy-assisted diffusion should not contribute to a great extent. This is due to the fact that vacancy creation at the most stable surface is energetically not a favorable process. Moreover, Li multiatom coordination inside the GB is a very favorable structure, leading to a more favorable hopping mechanism than any other mechanisms, which involves vacancy formation.

3.2.1. Li Diffusion through LiF/LiF GB. As shown in the previous section, there are two possible GB structures (Σ3 GB and Σ5 GB) for LiF/LiF. The migration of a Li atom in the vicinity of the Σ3 GB and Σ5 GB and parallel to the GB plane is studied. The simulation cell with the adatom is as shown in Figure 3a,b for Σ3 GB and Σ5 GB, respectively.

From the migration barriers as shown in Figure 3b,d, it could be seen that the barrier energy for Li to diffuse through the GB is lower in the case of the open Σ5 GB than the dense Σ3 GB. The energy barriers of 0.62 and 1.03 eV for open and dense structures show that the open structure allows for better diffusion through the GB than the dense structure. This might be due to lesser interaction from neighboring atoms in Σ5 GB.

3.2.2. Li Diffusion through Li_2O/Li_2O GB. This section examines Li diffusion in the simulation cell containing a Li_2O crystal with the Σ15 GB system as shown in Figure 4. In Figure 4a, the simulation cell used for the NEB calculation with the GB and the Li adatom placed at the GB region is shown. From Figure 4b, it could be seen that the migration barrier for Li diffusion through the GB structure is 0.78 eV, which suggests that the diffusion through this GB in Li_2O is slightly more hindered when compared to that of GBs in LiF.

3.2.3. Li Diffusion through LiF/Li_2O GB. This section reports Li diffusion in the simulation cell containing a Li_2O

DOI: 10.1021/acs.jpcc.9b00436
J. Phys. Chem. C 2019, 123, 10237−10245

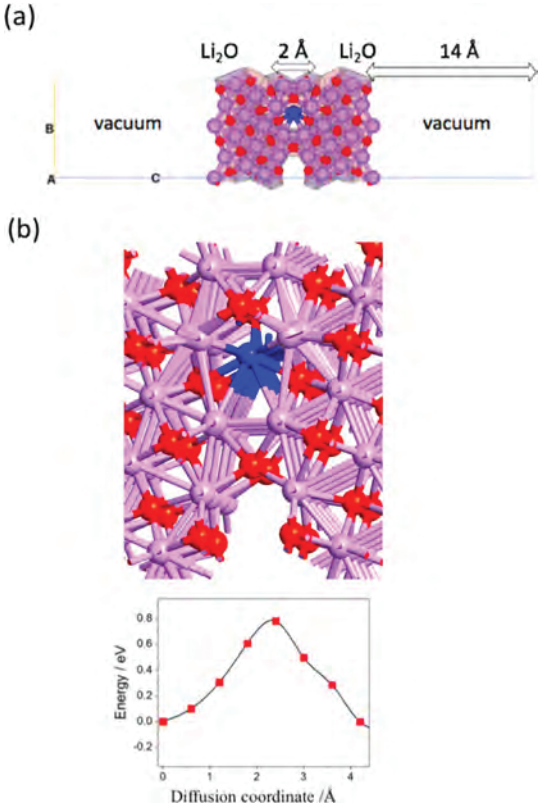

Figure 4. (a) Li_2O/Li_2O (210) GB (Σ15) with Li adatom (marked in blue). (b) Diffusion direction and migration barrier for Li_2O/Li_2O (310) GB (Σ15).

crystal on one side and LiF on the other with a GB interface. The migration of a Li atom in the vicinity of the GB and parallel to the GB plane is studied. However, unlike the case of LiF/LiF GBs or Li_2O/Li_2O GBs, in this structure there are different channels that could act as possible MEPs for Li diffusion. From Figure 5b–d, it could be seen that the migration barrier for Li diffusion through the GB structure ranges between 0.45 and 1 eV in the three paths and the MEP is as shown in Figure 5c and the migration barrier is 0.45 eV.

On the basis of all the evaluated values of migration barriers, the diffusion coefficients through all the GB systems are calculated and listed in Table 3. According to the results

Table 3. Summary of All Activation Energies and Diffusion Coefficients for Li Diffusion in the Respective GB

GB configuration	activation energy (eV)	pre-exponential factor (m^2/s)	diffusion coefficient (m^2/s)
LiF/LiF (Σ5 GB)	0.68	1.76×10^{-6}	4.6×10^{-16}
LiF/LiF (Σ3 GB)	1.03	1.23×10^{-6}	3.16×10^{-23}
Li_2O/Li_2O (Σ15 GB)	0.78	3.70×10^{-6}	7.38×10^{-16}
LiF/Li_2O	0.45	1.59×10^{-6}	3.87×10^{-14}

presented in Table 3, Li diffusion through the LiF/Li_2O GB is the most favorable mechanism because of the low energy barrier and a short diffusion distance. Physically, it occurs because of a multiatom hoping mechanism as discussed above. In this mechanism, Li is bonded to several different atoms while diffusing across the GB, which makes the diffusion process fast. It should be noted that the diffusion coefficients are calculated based on the Arrhenius equation (eq 3) assuming the attempt frequency of the first-order reaction (the order of the Debye frequency). In addition, the tracer correlation factor is set to one for simplicity. All of these factors

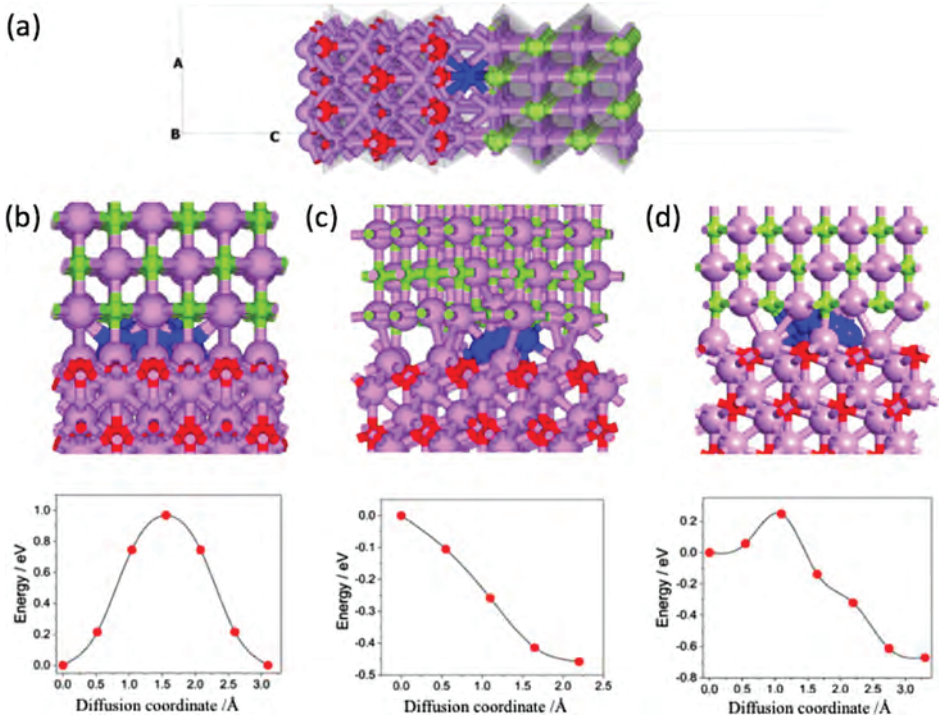

Figure 5. (a) LiF/Li_2O GB with Li adatom (marked in blue). (b) Diffusion direction (path 1) and migration barrier for LiF/Li_2O GB. (c) Diffusion direction (path 2) and migration barrier for LiF/Li_2O GB. (d) Diffusion direction (path 3) and migration barrier for LiF/Li_2O GB.

DOI: 10.1021/acs.jpcc.9b00436
J. Phys. Chem. C 2019, 123, 10237−10245

could potentially alter the diffusion coefficient values of Li in the GB. The diffusion dimensionality in each GB system is different. In the case of LiF/LiF GBs (both Σ5 and Σ3), the dimensionality of Li diffusion is 1 owing to the straight path of diffusion, whereas in the case of Li_2O/Li_2O GB, it is 2 and for LiF/Li_2O, it is 2 or 3 depending on the path.

Putting together the information regarding individual components in the SEI provides us an improved overall picture of transport through these complex interphases and their connection to the battery performance. Thus, we further compare our calculated energy barriers and the diffusion coefficients with those taken from the prior literature. In particular, we compare Li diffusion through the GB with the corresponding diffusion rate in the single components, which create the GB.

In the work of Chen et al.[31] the calculated Li migration energy barriers from DFT, along the major diffusion pathways of the three main components, LiF, Li_2O, and Li_2CO_3, were 0.73 eV, 0.152−1.362 eV, and 0.227−0.491 eV, respectively. Similar results for the energy barrier were found in the other DFT studies, where the lithium dynamics through LiF is investigated.[24,54] One of the most reported inorganic components that is found in the SEI is LiF.[24,25,31,54,55] Yildrim et al.[24] reported that the positively charged ion diffusivity in LiF is much lower than that in the other SEI inorganic components and suggested that diffusion in LiF is very slow, causing rate limitations in Li-ion diffusion. They used the DFT calculations to determine diffusion pathways and NEB method to calculate energy barriers of diffusion. They found that in the bulk of LiF, diffusion of vacancies is energetically more favorable than interstitials, and reported energy barriers of 0.73 and 1.09 eV for neutral vacancies and neutral Schottky vacancies, respectively, and the associated diffusion coefficients were reported in the order of 10^{-26} to -10^{-20} m^2/s. Recent studies, using the phase-field model together with Fick's law,[56] report a diffusion coefficient of Li in LiF at room temperatures (298−318 K) in the range of 3.7×10^{-16} m^2/s. Through our current DFT study with the GB structures of LiF, we determine that the migration energy barrier for Li-ion diffusion through the GB structure was 0.68 eV for Σ5 GB and 1.03 eV for Σ3 GB, which corresponds to diffusion coefficients of 4.60×10^{-16} m^2/s and 3.16×10^{-23} m^2/s, respectively. The diffusion coefficient values fall within the range of 10^{-26} to -10^{-16} m^2/s, which have been reported in different phase-field, molecular dynamics and NEB methods for the diffusion of Li in LiF. Considering the broad range of diffusion coefficients reported in the prior literature, we can conclude that our results indicate that Li diffusion through the LiF/LiF GB is faster or comparable to that of a pure grain.

In the case of Li_2O, only a very few theoretical studies reported the diffusion barriers through their bulk structures at low temperature.[31,57] Tasaki et al.[55] studied the diffusion of Li_2O and found transport coefficients in the range of 1.7×10^{-16} m^2/s. The current DFT results as shown in Table 3 suggest that the diffusion through the Li_2O/Li_2O GB system is at least 1 order of magnitude faster than that of the bulk structures of Li_2O.

There are no existing theoretical studies to compare the polycrystalline GB system that is considered in our current study. However, on comparing the values of diffusion coefficients obtained for the LiF/Li_2O GB system against the bulk LiF and the bulk Li_2O from the prior literature, we can see that there is a significant increase in the diffusion coefficient for the diffusion through the LiF/Li_2O GB system forming the rate-determining step in the diffusion process.

Experimentally, it is reported that the activation energy for lithium diffusion in the SEI ranges from 0.37 to 0.67 eV.[58−60] However, this value is very sensitive toward factors such as the charge/discharge state, the operating temperature, the content of the electrolyte, and so forth.[58,59] Therefore, quantitative comparison of the experimental data with our calculated energy barrier is not possible. However, qualitatively, our data are in good agreement with the experimental findings. Furthermore, as the energy barrier for lithium diffusion in LiF is substantially higher than in Li_2CO_3 and Li_2O, it is reasonable to conclude that the low lithium electrodeposited amount could be a side evidence of more LiF in the SEI when other conditions are similar.

Because the rate-determining step in the diffusion process is the diffusion through the GB, sub nanometer-sized particles of the Li metal can grow in these atomic length scale gaps in the GB, resulting in the nucleation of lithium filaments that may cause subsequent growth of dendrites under adverse conditions. This observation is also consistent with the fact that applying pressure or a mechanical barrier reduces the void spaces and improves the performance of Li metal anodes.[61]

4. SUMMARY AND CONCLUSIONS

The SEI growth rate, structure, composition, and resistance significantly depend upon the electrolyte composition. Furthermore, the distribution of intercalated/electrodeposited Li greatly depends on the SEI structure, which defines the subsequent electric potential gradient and the stress field.[62] Thus, the understanding of the Li diffusion mechanism and its energetics through the SEI is of imperative importance to understand and improve the performance of Li batteries. For that reason, in this work, we employ the first-principles calculations based on DFT to investigate different aspects of Li atom diffusion through the GB of the SEI. In this work, we consider the most studied, however, not greatly understood SEI of LIBs and LMBs. In particular, five different GB structures are investigated, and their interface atomic and electronic structures are carefully analyzed. It is revealed that the LiF/LiF, Li_2O/Li_2O, and LiF/Li_2O GBs are the most stable configurations. Subsequently, the Li diffusion mechanism and energetics through these stable GB interfaces are investigated. Among the studied GBs, the fastest Li diffusion rate is observed for the heterogeneous LiF/Li_2O GB, compared to the homogeneous LiF/LiF and Li_2O/Li_2O. This is due to the fact that Li multiatom coordination inside the GB is a very favorable structure, leading to the multiatom hopping mechanism that is more advantageous than any other mechanisms.

Because little is known about the actual structure and configuration of the GB in the SEI of operating cells, the presently investigated GB for the Li diffusion might be simpler than the real-cell structures. For example, numerous defects and/or impurities could exist in the local structure of the SEI, which could potentially influence Li diffusivity. In addition, there are other external factors that could influence Li diffusivity in the SEI, such as an applied electric field and temperature.[58] However, it is expected that these external factors would influence Li diffusion through the GB in the same way as through the respective grains.

Nevertheless, the relatively low DFT computational cost using the GB configuration of 200−300 atoms enables a broad

DOI: 10.1021/acs.jpcc.9b00436
J. Phys. Chem. C 2019, 123, 10237−10245

range of parametric studies that could suggest new and/or improved strategies for Li dendrite formation and growth in the case of LMBs. Moreover, it is common in the higher hierarchy cell-level models to represent the SEI as a constant resistance ignoring its chemistry and transport properties. However, incorporating the details of the ion diffusion and the detailed SEI chemistry into battery cell-level models, in a more fundamental manner, could enable the profound investigation of the SEI influence on battery performance and efficiency. Thus, the results from the present work, in addition to revealing the diffusion mechanism of Li in the GB of the SEI, are a step forward toward more robust cell models.

■ ASSOCIATED CONTENT

Supporting Information

The Supporting Information is available free of charge on the ACS Publications website at DOI: 10.1021/acs.jpcc.9b00436.

Details of the bulk crystal structure, minimum energy surface slabs, and hopping mechanism of Li diffusion through the GB structures (PDF)

■ AUTHOR INFORMATION

Corresponding Author

*E-mail: mashayek@uic.edu. Phone: +1 (312) 996 1154.

ORCID

Ajaykrishna Ramasubramanian: 0000-0003-3005-6665

Vitaliy Yurkiv: 0000-0002-3407-891X

Tara Foroozan: 0000-0003-1334-3048

Reza Shahbazian-Yassar: 0000-0002-7744-4780

Notes

The authors declare no competing financial interest.

■ ACKNOWLEDGMENTS

The authors acknowledge the financial support from the National Science Foundation award CBET-1805938. In addition, the authors would like to acknowledge the Advanced Cyberinfrastructure for Education and Research (ACER) group at The University of Illinois at Chicago (URL: https://acer.uic.edu) as well as the National Science Foundation Extreme Science and Engineering Discovery Environment (XSEDE) award no. TG-DMR180106 for providing HPC resources that have contributed to the research results reported in this paper.

■ REFERENCES

(1) Scrosati, B.; Hassoun, J.; Sun, Y.-K. Lithium-Ion Batteries. A Look into the Future. *Energy Environ. Sci.* **2011**, *4*, 3287−3295.

(2) Thackeray, M. M.; Wolverton, C.; Isaacs, E. D. Electrical Energy Storage for Transportation− Approaching the Limits of, and Going Beyond, Lithium-Ion Batteries. *Energy Environ. Sci.* **2012**, *5*, 7854−7863.

(3) Yu, X.; Manthiram, A. Electrode-Electrolyte Interfaces in Lithium-Based Batteries. *Energy Environ. Sci.* **2018**, *11*, 527−543.

(4) Cheng, X.-B.; Zhang, R.; Zhao, C.-Z.; Wei, F.; Zhang, J.-G.; Zhang, Q. A Review of Solid Electrolyte Interphases on Lithium Metal Anode. *Adv. Sci.* **2015**, *3*, 1500213.

(5) Yan, C.; Cheng, X.-B.; Zhao, C.-Z.; Huang, J.-Q.; Yang, S.-T.; Zhang, Q. Lithium Metal Protection through in Situ Formed Solid Electrolyte Interphase in Lithium-Sulfur Batteries: The Role of Polysulfides on Lithium Anode. *J. Power Sources* **2016**, *327*, 212−220.

(6) Yurkiv, V.; Foroozan, T.; Ramasubramanian, A.; Shahbazian-Yassar, R.; Mashayek, F. Phase-Field Modeling of Solid Electrolyte Interface (SEI) Influence on Li Dendritic Behavior. *Electrochim. Acta* **2018**, *265*, 609−619.

(7) Peled, E. The Electrochemical Behavior of Alkali and Alkaline Earth Metals in Nonaqueous Battery Systems-The Solid Electrolyte Interphase Model. *J. Electrochem. Soc.* **1979**, *126*, 2047−2051.

(8) Peled, E.; Golodnttsky, D.; Ardel, G.; Menachem, C.; Bar Tow, D.; Eshkenazy, V. The Role of Sei in Lithium and Lithium Ion Batteries. *MRS Proc* **1995**, *393*, 209−219.

(9) Peled, E.; Menachem, C.; Bar Tow, D.; Melman, A. Improved Graphite Anode for Lithium-Ion Batteries Chemically. *J. Electrochem. Soc.* **1996**, *143*, L4−L7.

(10) Peled, E.; Golodnitsky, D.; Ardel, G. Advanced Model for Solid Electrolyte Interphase Electrodes in Liquid and Polymer Electrolytes. *J. Electrochem. Soc.* **1997**, *144*, L208−L210.

(11) Broussely, M.; Biensan, P.; Bonhomme, F.; Blanchard, P.; Herreyre, S.; Nechev, K.; Staniewicz, R. J. Main Aging Mechanisms in Li Ion Batteries. *J. Power Sources* **2005**, *146*, 90−96.

(12) Vetter, J.; Novák, P.; Wagner, M. R.; Veit, C.; Möller, K.-C.; Besenhard, J. O.; Winter, M.; Wohlfahrt-Mehrens, M.; Vogler, C.; Hammouche, A. Ageing Mechanisms in Lithium-Ion Batteries. *J. Power Sources* **2005**, *147*, 269−281.

(13) Zhang, H.-L.; Li, F.; Liu, C.; Tan, J.; Cheng, H.-M. New Insight into the Solid Electrolyte Interphase with Use of a Focused Ion Beam. *J. Phys. Chem. B* **2005**, *109*, 22205−22211.

(14) Verma, P.; Maire, P.; Novák, P. Electrochimica Acta Review Article A Review of the Features and Analyses of the Solid Electrolyte Interphase in Li-Ion Batteries. *Electrochim. Acta* **2010**, *55*, 6332−6341.

(15) Smith, A. J.; Burns, J. C.; Zhao, X.; Xiong, D.; Dahn, J. R. A High Precision Coulometry Study of the SEI Growth in Li/graphite Cells. *J. Electrochem. Soc.* **2011**, *158*, A447−A452.

(16) Edström, K.; Herstedt, M.; Abraham, D. P. A New Look at the Solid Electrolyte Interphase on Graphite Anodes in Li-Ion Batteries. *J. Power Sources* **2006**, *153*, 380−384.

(17) Lu, M.; Cheng, H.; Yang, Y. A Comparison of Solid Electrolyte Interphase (SEI) on the Artificial Graphite Anode of the Aged and Cycled Commercial Lithium Ion Cells. *Electrochim. Acta* **2008**, *53*, 3539−3546.

(18) Cresce, A. V.; Russell, S. M.; Baker, D. R.; Gaskell, K. J.; Xu, K. In Situ and Quantitative Characterization of Solid Electrolyte Interphases. *Nano Lett.* **2014**, *14*, 1405−1412.

(19) Shi, S.; Lu, P.; Liu, Z.; Qi, Y.; Hector, L. G.; Li, H.; Harris, S. J. Direct Calculation of Li-Ion Transport in the Solid Electrolyte Interphase. *J. Am. Chem. Soc.* **2012**, *134*, 15476−15487.

(20) Aurbach, D.; Markovsky, B.; Levi, M. D.; Levi, E.; Schechter, A.; Moshkovich, M.; Cohen, Y. New Insights into the Interactions between Electrode Materials and Electrolyte Solutions for Advanced Nonaqueous Batteries. *J. Power Sources* **1999**, *81-82*, 95−111.

(21) Wang, A.; Kadam, S.; Li, H.; Shi, S.; Qi, Y. Review on Modeling of the Anode Solid Electrolyte Interphase (SEI) for Lithium-Ion Batteries. *npj Comput. Mater.* **2018**, *4*, 15.

(22) Tarascon, J.-M.; Armand, M. Issues and Challenges Facing Rechargeable Lithium Batteries. *Nature* **2001**, *414*, 359−367.

(23) Shi, S.; Gao, J.; Liu, Y.; Zhao, Y.; Wu, Q.; Ju, W.; Ouyang, C.; Xiao, R. Multi-Scale Computation Methods: Their Applications in Lithium-Ion Battery Research and Development. *Chin. Phys. B* **2016**, *25*, 018212.

(24) Yildirim, H.; Kinaci, A.; Chan, M. K. Y.; Greeley, J. P. First-Principles Analysis of Defect Thermodynamics and Ion Transport in Inorganic SEI Compounds : LiF and NaF. *ACS Appl. Mater. Interfaces* **2015**, *7*, 18985−18996.

(25) Liu, Z.; Qi, Y.; Lin, Y. X.; Chen, L.; Lu, P.; Chen, L. Q. Interfacial Study on Solid Electrolyte Interphase at Li Metal Anode: Implication for Li Dendrite Growth. *J. Electrochem. Soc.* **2016**, *163*, A592−A598.

(26) Shi, S.; Zhang, H.; Ke, X.; Ouyang, C.; Lei, M.; Chen, L. First-Principles Study of Lattice Dynamics of $LiFePO_4$. *Phys. Lett. A* **2009**, *373*, 4096−4100.

(27) Zhao, Q.; Pan, L.; Li, Y.-J.; Chen, L.-Q.; Shi, S.-Q. Rotational Motion of Polyanion versus Volume Effect Associated with Ionic

Conductivity of Several Solid Electrolytes. *Rare Met.* **2018**, *37*, 497−503.
(28) Benitez, L.; Cristancho, D.; Seminario, J. M.; Martinez de la Hoz, J. M.; Balbuena, P. B.; Tarascon, J. M.; Armand, M. Electron Transfer through Solid-Electrolyte-Interphase Layers Formed on Si Anodes of Li-Ion Batteries. *Electrochim. Acta* **2014**, *140*, 250−257.
(29) Shi, S.; Qi, Y.; Li, H.; Hector, L. G. Defect Thermodynamics and Diffusion Mechanisms in Li_2CO_3 and Implications for the Solid Electrolyte Interphase in Li-Ion Batteries. *J. Phys. Chem. C* **2013**, *117*, 8579−8593.
(30) Soto, F. A.; Marzouk, A.; El-Mellouhi, F.; Balbuena, P. B. Understanding Ionic Diffusion through SEI Components for Lithium-Ion and Sodium-Ion Batteries: Insights from First-Principles Calculations. *Chem. Mater.* **2018**, *30*, 3315−3322.
(31) Chen, Y. C.; Ouyang, C. Y.; Song, L. J.; Sun, Z. L. Electrical and Lithium Ion Dynamics in Three Main Components of Solid Electrolyte Interphase from Density Functional Theory Study. *J. Phys. Chem. C* **2011**, *115*, 7044−7049.
(32) Christensen, J.; Newman, J. A Mathematical Model for the Lithium-Ion Negative Electrode Solid Electrolyte Interphase. *J. Electrochem. Soc.* **2004**, *151*, A1977−A1988.
(33) Leung, K.; Jungjohann, K. L. Spatial Heterogeneities and Onset of Passivation Breakdown at Lithium Anode Interfaces. *J. Phys. Chem. C* **2017**, *121*, 20188−20196.
(34) Kresse, G.; Furthmüller, J. Efficient iterative schemes forab initiototal-energy calculations using a plane-wave basis set. *Phys. Rev. B: Condens. Matter Mater. Phys.* **1996**, *54*, 11169−11186.
(35) Blöchl, P. E. Projector Augmented-Wave Method. *Phys. Rev. B: Condens. Matter Mater. Phys.* **1994**, *50*, 17953−17979.
(36) Perdew, J. P.; Ruzsinszky, A.; Csonka, G. I.; Vydrov, O. A.; Scuseria, G. E.; Constantin, L. A.; Zhou, X.; Burke, K. Restoring the Density-Gradient Expansion for Exchange in Solids and Surfaces. *Phys. Rev. Lett.* **2008**, *100*, 136406−136411.
(37) Perdew, J. P.; Burke, K.; Ernzerhof, M. Generalized Gradient Approximation Made Simple. *Phys. Rev. Lett.* **1996**, *77*, 3865−3868.
(38) Henkelman, G.; Uberuaga, B. P.; Jónsson, H.; Henkelman, G. A Climbing Image Nudged Elastic Band Method for Finding Saddle Points and Minimum Energy Paths. *J. Chem. Phys.* **2000**, *113*, 9901.
(39) Mouhat, F.; Coudert, F. X. Necessary and Sufficient Elastic Stability Conditions in Various Crystal Systems. *Phys. Rev. B: Condens. Matter Mater. Phys.* **2014**, *90*, 224104.
(40) Lenchuk, O.; Rohrer, J.; Albe, K. Cohesive Strength of Zirconia/molybdenum Interfaces and Grain Boundaries in Molybdenum: A Comparative Study. *Acta Mater.* **2017**, *135*, 150−157.
(41) Yu, R.; Zhu, J.; Ye, H. Q. Calculations of Single-Crystal Elastic Constants Made Simple. *Comput. Phys. Commun.* **2010**, *181*, 671−675.
(42) Panahian Jand, S.; Kaghazchi, P. The Role of Electrostatic Effects in Determining the Structure of LiF-Graphene Interfaces. *J. Phys.: Condens. Matter* **2014**, *26*, 262001.
(43) Radin, M. D.; Rodriguez, J. F.; Tian, F.; Siegel, D. J. Lithium Peroxide Surfaces Are Metallic, While Lithium Oxide Surfaces Are Not. *J. Am. Chem. Soc.* **2012**, *134*, 1093−1103.
(44) Bruno, M.; Prencipe, M. Ab initio quantum-mechanical modeling of the (001), and (110) surfaces of zabuyelite (Li2CO3). *Surf. Sci.* **2007**, *601*, 3012−3019.
(45) Nie, M.; Chalasani, D.; Abraham, D. P.; Chen, Y.; Bose, A.; Lucht, B. L. Lithium Ion Battery Graphite Solid Electrolyte Interphase Revealed by Microscopy and Spectroscopy. *J. Phys. Chem. C* **2013**, *117*, 1257−1267.
(46) Nie, M.; Abraham, D. P.; Chen, Y.; Bose, A.; Lucht, B. L. Silicon Solid Electrolyte Interphase (SEI) of Lithium Ion Battery Characterized by Microscopy and Spectroscopy. *J. Phys. Chem. C* **2013**, *117*, 13403−13412.
(47) Parimalam, B. S.; MacIntosh, A. D.; Kadam, R.; Lucht, B. L. Decomposition Reactions of Anode Solid Electrolyte Interphase (SEI) Components with LiPF6. *J. Phys. Chem. C* **2017**, *121*, 22733−22738.
(48) Santoro, A.; Mighell, A. D. Coincidence-site lattices. *Acta Crystallogr., Sect. A: Cryst. Phys., Diffr., Theor. Gen. Crystallogr.* **1973**, *29*, 169−175.
(49) *Atomistix Toolkit*, version 2016.4; Synopsys QuantumWise A/S, 2016.
(50) Stradi, D.; Jelver, L.; Smidstrup, S.; Stokbro, K. Method for Determining Optimal Supercell Representation of Interfaces. *J. Phys.: Condens. Matter* **2017**, *29*, 185901.
(51) Schneider, J.; Hamaekers, J.; Chill, S. T.; Smidstrup, S.; Bulin, J.; Thesen, R.; Blom, A.; Stokbro, K. ATK-ForceField: a new generation molecular dynamics software package. *Modell. Simul. Mater. Sci. Eng.* **2017**, *25*, 085007.
(52) Smidstrup, S.; Pedersen, A.; Stokbro, K.; Jónsson, H. Improved Initial Guess for Minimum Energy Path Calculations. *J. Chem. Phys.* **2014**, *140*, 214106.
(53) Kim, H.; Windl, W. Efficient Ab-Initio Calculation of the Elastic Properties of Nanocrystalline Silicon. *J. Comput. Theor. Nanosci.* **2007**, *4*, 65−70.
(54) Fan, L.; Zhuang, H. L.; Gao, L.; Lu, Y.; Archer, L. A. Regulating Li Deposition at Artificial Solid Electrolyte Interphases. *J. Mater. Chem. A* **2017**, *5*, 3483−3492.
(55) Tasaki, K.; Goldberg, A.; Lian, J.; Walker, M.; Timmons, A.; Harris, S. J. Solubility of Lithium Salts Formed on the Lithium-Ion Battery Negative Electrode Surface in Organic Solvents. *J. Electrochem. Soc.* **2009**, *156*, A1019−A1027.
(56) Guan, P.; Liu, L.; Lin, X. Simulation and Experiment on Solid Electrolyte Interphase (SEI) Morphology Evolution and Lithium-Ion Diffusion. *J. Electrochem. Soc.* **2015**, *162*, A1798−A1808.
(57) Koyama, Y.; Yamada, Y.; Tanaka, I.; Nishitani, S. n. R.; Adachi, H.; Murayama, M.; Kanno, R. Evaluation of Migration Energy of Lithium Ions in Chalcogenides and Halides by First Principles Calculation. *Mater. Trans.* **2002**, *43*, 1460−1463.
(58) Churikov, A. V. Transfer Mechanism in Solid-Electrolyte Layers on Lithium: Influence of Temperature and Polarization. *Electrochim. Acta* **2001**, *46*, 2415−2426.
(59) Levi, M. D.; Wang, C.; Aurbach, D. Self-Discharge of Graphite Electrodes at Elevated Temperatures Studied by CV and Electrochemical Impedance Spectroscopy. *J. Electrochem. Soc.* **2004**, *151*, A781−A790.
(60) Schranzhofer, H.; Bugajski, J.; Santner, H. J.; Korepp, C.; Möller, K.-C.; Besenhard, J. O.; Winter, M.; Sitte, W. Electrochemical Impedance Spectroscopy Study of the SEI Formation on Graphite and Metal Electrodes. *J. Power Sources* **2006**, *153*, 391−395.
(61) Mikhaylik, Y. V.; Kovalev, I.; Schock, R.; Kumaresan, K.; Xu, J.; Affinito, J. High Energy Rechargeable Li-S Cells for EV Application: Status, Remaining Problems and Solutions. *ECS Trans.* **2009**, *25*, 23−34.
(62) Yurkiv, V.; Foroozan, T.; Ramasubramanian, A.; Shahbazian-Yassar, R.; Mashayek, F. The Influence of Stress Field on Li Electrodeposition in Li-Metal Battery. *MRS Commun.* **2018**, *8*, 1285−1291.

DOI: 10.1021/acs.jpcc.9b00436
J. Phys. Chem. C 2019, 123, 10237−10245